Monitoring the Characteristics of the Bohai Sea Ice Using High-Resolution Geostationary Ocean Color Imager (GOCI) Data

Yan, Yu

2019-02-01

Yan , Y , Huang , K , Shao , D , Xu , Y & Gu , W 2019 , ' Monitoring the Characteristics of the Bohai Sea Ice Using High-Resolution Geostationary Ocean Color Imager (GOCI) Data ' , Sustainability , vol. 11 , no. 3 , 777 . https://doi.org/10.3390/su11030777

http://hdl.handle.net/10138/300124
https://doi.org/10.3390/su11030777

sustainability

MDPI

Article

Monitoring the Characteristics of the Bohai Sea Ice Using High-Resolution Geostationary Ocean Color Imager (GOCI) Data

Yu Yan [1,2,3], Kaiyue Huang [1,3], Dongdong Shao [4,*], Yingjun Xu [1,3] and Wei Gu [1,3]

1 Key Laboratory of Environmental Change and Natural Disaster, Ministry of Education, Beijing Normal University, Beijing 100875, China; yu.yan@helsinki.fi (Y.Y.); huangky@mail.bnu.edu.cn (K.H.); xyj@bnu.edu.cn (Y.X.); weigu@bnu.edu.cn (W.G.)
2 Institute for Atmospheric and Earth System Research (INAR), Faculty of Science, University of Helsinki, 00014 Helsinki, Finland
3 Academy of Disaster Reduction and Emergency Management, Faculty of Geographical Science, Beijing Normal University, Beijing 100875, China
4 State Key Laboratory of Water Environment Simulation & School of Environment, Beijing Normal University, Beijing 100875, China
* Correspondence: ddshao@bnu.edu.cn; Tel.: +86-10-58805053

Received: 28 November 2018; Accepted: 30 January 2019; Published: 1 February 2019

Abstract: Satellite remote sensing data, such as moderate resolution imaging spectroradiometers (MODIS) and advanced very high-resolution radiometers (AVHRR), are being widely used to monitor sea ice conditions and their variability in the Bohai Sea, the southernmost frozen sea in the Northern Hemisphere. Monitoring the characteristics of the Bohai Sea ice can provide crucial information for ice disaster prevention for marine transportation, oil field operation, and regional climate change studies. Although these satellite data cover the study area with fairly high spatial resolution, their typically limited cloudless images pose serious restrictions for continuous observation of short-term dynamics, such as sub-seasonal changes. In this study, high spatiotemporal resolution (500 m and eight images per day) geostationary ocean color imager (GOCI) data with a high proportion of cloud-free images were used to monitor the characteristics of the Bohai Sea ice, including area and thickness. An object-based feature extraction method and an albedo-based thickness inversion model were used for estimating sea ice area and thickness, respectively. To demonstrate the efficacy of the new dataset, a total of 68 GOCI images were selected to analyze the evolution of sea ice area and thickness during the winter of 2012–2013 with severe sea ice conditions. The extracted sea ice area was validated using Landsat Thematic Mapper (TM) data with higher spatial resolution, and the estimated sea ice thickness was found to be consistent with in situ observation results. The entire sea ice freezing–melting processes, including the key events such as the day with the maximum ice area and the first and last days of the frozen season, were better resolved by the high temporal-resolution GOCI data compared with MODIS or AVHRR data. Both characteristics were found to be closely correlated with cumulative freezing/melting degree days. Our study demonstrates the applicability of the GOCI data as an improved dataset for studying the Bohai Sea ice, particularly for purposes that require high temporal resolution data, such as sea ice disaster monitoring.

Keywords: sea ice monitoring; geostationary ocean color imager; ocean remote sensing; Bohai Sea

1. Introduction

The Bohai Sea is a semi-enclosed sea located at approximately 117°–122° E, 37°–41° N in North China (Figure 1). It freezes every winter for about three to four months from December to the next

March, and is the southernmost frozen sea in the Northern Hemisphere. The Bohai Sea possesses rich fishery, oil, and gas resources, making the Bohai Rim a critical economic zone in China [1]. Subject to global and regional climate changes, sea ice extent exhibits heterogeneous variability across the globe [2–5]. While a significant decreasing trend of Arctic sea ice extent since the 1980s has been observed, sea ice extent has showed significant and slight increasing trends in the Antarctic and the Bohai Sea, respectively [4,5]. Varying Bohai Sea ice conditions severely influence marine navigation, offshore oil exploitation, mariculture, and coastal construction [1,6,7]. Sea ice can be desalinated using proper techniques to produce freshwater for industrial and agricultural consumption, with the potential to become an alternative freshwater resource that may help alleviate the severe freshwater shortage in the region [8–10]. Therefore, the ability to closely monitor the sea ice conditions and their variability in this region is critical for ice disaster prevention, climate change studies, and sea ice resource estimation.

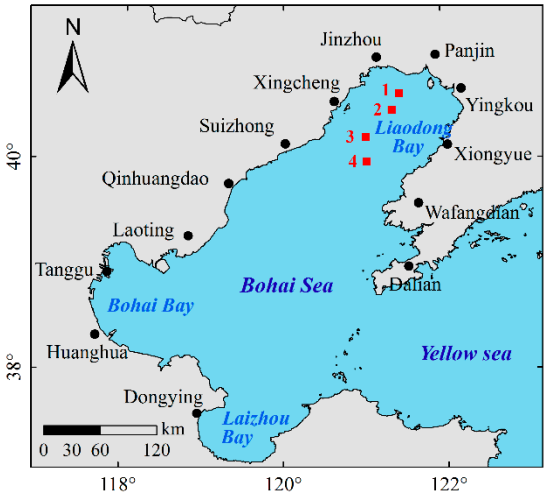

Figure 1. Location of the Bohai Sea. The black dots represent the 13 meteorological stations. The red squares represent the oil platforms where the in situ measurements of sea ice thickness were conducted.

Satellite remote sensing data have been widely applied to investigate the spatiotemporal distribution and evolution of sea ice. Particularly, polar-orbiting satellites, such as the Earth Observing System (EOS) moderate-resolution imaging spectroradiometer (MODIS) and the National Oceanic and Atmospheric Administration (NOAA) advanced very high-resolution radiometer (AVHRR), have been commonly used to study the Bohai Sea ice [5,9,11–16]. Although these satellite data cover the study area with a fairly high spatial resolution (~1 km), they are typically limited in temporal resolution and provide only one image covering the study area per day, which are constrained by the proportion of cloud-free images of the MODIS and the AVHRR data being mostly less than 20% [5,15]. Synthetic aperture radar (SAR) data is also commonly used to monitor sea ice, which has also been applied to detecting ice types and thickness in the Bohai Sea due to their fine spatial resolution and insensitivity to cloud interference [17–19]. However, the SAR data are limited by a long repeat cycle (6–44 days) [20]. As such, these data are not suitable for continuous observation of short-term dynamics, such as the sub-seasonal changes.

The first geostationary ocean color imager (GOCI) in the world was launched on June 27, 2010, providing a stationary observation of a zone of 2500 km × 2500 km around the Korean Peninsula [21], which covers the Bohai Sea. GOCIs produce eight images at a 500 m spatial resolution and hourly interval from 8:15 a.m. to 3:45 p.m. local time every day, and the images cover eight spectral bands with blue to near-infrared wavelengths [22]. Due to their wide coverage and high spatiotemporal resolution, the GOCI data have been used to study the optical characteristics of water [21,23,24], ocean surface currents [25–28], biological features of waters [29–31], water quality [32–34], harmful algal bloom [35,36], sea surface salinity [37], and sea fog [38]. However, these high-quality data have not yet

been applied to the characteristics of Bohai Sea ice, where fast-changing first-year ice poses challenges for traditional satellites.

In this study, high-spatiotemporal resolution GOCI data with high proportions of cloud-free images were applied to monitor the characteristics of Bohai Sea ice, including area and thickness. To demonstrate the efficacy of the new dataset, the winter of 2012–2013 was chosen as a case study period, as severe ice conditions appeared in the Bohai Sea during this period. Section 2 introduces the study area. Section 3 describes the remote sensing data and relevant meteorological data, as well as the methodologies used to extract sea ice area and thickness. Section 4 presents the results on the evolution of sea ice area and thickness during the winter of 2012–2013, as well as their correlation with meteorological factors, which is followed by a discussion of the benefits of using the new dataset in Section 5. Our main conclusions are listed in Section 6.

2. Study Area

The Bohai Sea is a semi-enclosed sea covering 73,686 km^2 in Northern China, consisting of Liaodong Bay, Bohai Bay, Laizhou Bay, and the central Bohai Sea, and is connected to the Yellow Sea to the east (Figure 1). Several major cities are located along the Bohai Sea coast, including Tianjin, Dalian, Yingkou, Jinzhou, Qinhuangdao, and Dongying. The major tributaries include the Yellow River, Hai River, Liao River, and Luan River, which carry large amounts of freshwater and sediments from land to the Bohai Sea. The average water depth of the Bohai Sea is 18 m. The salinity of the seawater is only 30 PSU, which is the lowest among all Chinese coastal water [14]. The mean surface water temperature ranges from 0 °C (February) to 21 °C (August) [11]. The frozen period of the Bohai Sea is generally from early December to mid-March.

3. Data and Methods

3.1. Data Description

3.1.1. Remote Sensing Data

GOCI Level 1B (L1B) data were downloaded from the Korea Ocean Satellite Center (KOSC) [39]. The GOCI image covers eight spectral bands, including six visible bands and two near-infrared bands, as shown in Table 1. To study the daily variation of sea ice, we are aiming to obtain one best image out of eight available ones for each day from 1 December 2012 to 31 March 2013. The criterion of selection is to pick the one with least disturbances from cloud cover, sea fog cover, uneven illumination, and dislocation. A total of 73 images were selected to cover 73 days, while no clear images were available for the other days.

Table 1. The parameters of the spectral bands of geostationary ocean color imager (GOCI) images.

Band	Central Wavelengths (nm)	Bandwidth (nm)	Nominal Radiance ($W \cdot m^{-2} \cdot um^{-1} \cdot sr^{-1}$)	Saturation Radiance ($W \cdot m^{-2} \cdot um^{-1} \cdot sr^{-1}$)
1	412	20	100.0	150.0
2	443	20	92.5	145.8
3	490	20	72.2	115.5
4	555	20	55.3	85.2
5	660	20	32.0	58.3
6	680	10	27.1	46.2
7	745	20	17.7	33.0
8	865	40	12.0	23.4

Landsat Thematic Mapper (TM) and MODIS data were also used for validation and comparison purposes in this study. Landsat TM data with 30 m spatial resolutions were obtained from the U.S. Geological Survey (USGS) website [40], and the Chinese mirror website is in the Geospatial Data Cloud website [41]. During the chosen study period, the TM image was cloudless only on 22 December 2012,

which was thus selected for validation. A total of 106 Terra MODIS images with spatial resolutions of 500 m were downloaded from the National Aeronautics and Space Administration (NASA) Level 1 and Atmosphere Archive and Distribution System (LAADS) website [42], among which 15 cloud-free images were selected.

3.1.2. Meteorological Data

Daily meteorological data, including the minimum, average, and maximum daily temperatures at 13 meteorological stations (Jinzhou, Panjin, Yingkou, Xingcheng, Xiongyue, Suizhong, Qinhuangdao, Wafangdian, Laoting, Dalian, Tanggu, Huanghua, and Dongying) surrounding the Bohai Sea, were obtained from the website of the National Meteorological Information Center of China [43] during the entire study period. The average daily temperature data were further applied to calculate cumulative freezing degree days (CFDD) and cumulative melting degree days (CMDD) in Section 3.5.

3.1.3. In Situ Measurement of Sea Ice Thickness

In situ observed sea ice thickness data in the winter of 2012–2013 were obtained from the literature [19] for validation. The locations of the observed stations are shown in Figure 1. The numbers 1–4 labelled in Figure 1 represent the four offshore oil platforms of JZ09–3, JZ20–2, JZ25–1, and JX01-1, respectively, in this study. The samples shown here were evenly distributed in January and February (January 2, 6, 9, 16, and 26; and February 2, 9, 12, and 16).

3.2. GOCI Data Pre-Processing

The pre-processing of the GOCI data primarily included three steps: Radiometric calibration, geometric correction, and atmospheric correction. The process of radiometric calibration of the GOCI data involved converting the L1B data from digital numbers to radiance units using ENVI 5.1 (ITT Visual Information Solutions, Boulder, CO, USA). The Geographic Lookup Table (GLT) method [44] was used for geometric correction of GOCI data to provide the actual location of an uncorrected pixel in the output.

In order to accurately derive the surface reflectance, atmospheric correction is required for eliminating the absorption effect of solar shortwave radiation [45]. As a relatively new remote sensing dataset, there is no well-established algorithm for an atmospheric correction for GOCI. In this study, the Fast Line-of-Sight Atmospheric Analysis of Spectral Hypercube (FLAASH) atmospheric correction method [14] was used for GOCI data. FLAASH has been widely applied for multi-band or hyperspectral data [5,46], including an aerosol estimation algorithm considering the dark pixel reflectance ratio, to remove atmospheric scattering and absorption in the 400–2500 nm wavelength range. The input parameters for FLAASH atmospheric correction for a sample GOCI image are listed in Table 2. After conducting a set of iterative calculations to quantify water and aerosol amounts, we obtained atmospherically corrected images with units of apparent surface reflectance.

Table 2. Input parameters for Fast Line-of-Sight Atmospheric Analysis of Spectral Hypercube (FLAASH) atmospheric correction for a sample GOCI image.

Sensor Altitude	**Ground Elevation**	**Pixel Size**	**Flight Date**	**Flight Time (GMT)**
35,786 km	0 m	500 m	2013–02–01	06:16:43
Atmospheric model	**Aerosol model**	**Water column multiplier**	**Initial visibility**[1]	**CO_2 mixing ratio**
Mid-latitude winter	Maritime	1.0	18.6 km	390 ppm

[1] The initial visibility data was obtained from the Wunderground website [47].

3.3. Extraction of Sea Ice Area

The desired sea ice features were extracted from the GOCI image using an object-based feature extraction method [5,48–50]. Before using the object-based feature extraction method, we used a land mask of the Bohai Sea to mask the land in the pre-processed images. Then, the image was segmented and neighboring pixels of a number of objects were grouped based on the similarity of spectral and texture characteristics [50]. During the process of segmentation, a merge level (usually 60–80) was set to avoid over-segmentation and improve the integrity of sea ice information by combining the speckles with identical features [49]. After segmentation, the workflow of an example-based feature extraction in Environment for Visualizing Images (ENVI) 5.1 (ITT Visual Information Solutions, Boulder, CO, USA) was used to discriminate the sea ice from sea water and thick cloud. Specifically, for each image, we manually selected representative objects of seawater, sea ice and thick cloud (if existing) based on visual interpretation, then computed the spectral, texture, and spatial attributes of these sample objects to define classifications, which were used for feature extraction and outputted as shapefiles. Finally, the output shapefiles were further corrected using visual interpretation in ArcGIS 10.1 (Esri, Redlands, CA, USA), e.g., removing polygons incorrectly classified as sea ice and vice versa [5,50]. Notably, the light clouds were manually removed in this step by repeating a manual cloud masking through visual interpretation [51], as it was difficult to distinguish between sea ice and light clouds using the above method and the area of the clouds was usually small. The selected 68 pre-processed images were processed step-by-step as described above to obtain the sea ice area. Figure 2 shows an example of the sea ice area extracted through the object-based feature extraction method. The above method was further applied for TM and MODIS data to extract sea ice area.

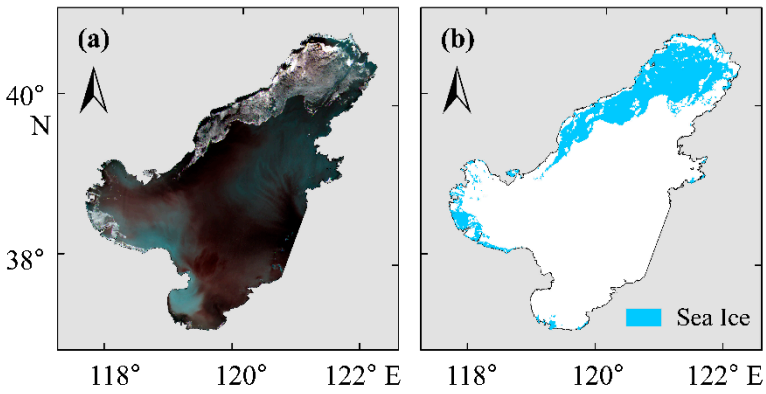

Figure 2. Bohai Sea ice area extraction: (**a**) The original image using bands 6/5/4 (680/660/555 nm, respectively) (February 1, 2013) and (**b**) the blue-color-coded sea ice area extracted using the object-based feature extraction method.

3.4. Sea Ice Thickness Inversion

Numerous studies [11,52,53] have stated that sea ice thickness is strongly related to its surface albedo, which leads to the sea ice thickness inversion model, i.e., the exponential relationship between sea ice thickness and its albedo derived from remote sensing data [11,14,15,54,55]:

$$h = -\ln[(1 - \alpha_h \cdot {\alpha_{max}}^{-1}) \cdot k^{-1}] \cdot {\mu_\alpha}^{-1}, \quad (1)$$

where h is the sea ice thickness; α_h is the sea ice albedo of solar shortwave radiation; α_{max} is the albedo corresponding to infinite ice thickness; k is a correlation coefficient related to α_{max} and α_{sea}, i.e., $k = 1 - \alpha_{sea}/\alpha_{max}$, where α_{sea} is the albedo of seawater; and μ_α (m^{-1}) is the attenuation coefficient of the albedo. The parameters of α_{max}, α_{sea}, and μ_α all assumed values obtained from field experiments in previous studies [11,14,15,54,55], setting to 0.70, 0.06, and 2.6599, respectively. In this study, the effects of snow were neglected and Equation (1) was used to estimate the bare sea ice thickness under the

assumption that no snow cover exists, as the amount of snowfall in the Bohai Sea during the winter is generally minimal [56]. Even when snowfall occurs, snow cover is still limited on the sea ice due to the effects of wind and current [56,57]. The effects of surface melt were also neglected as the meltwater layers on ice surfaces were extremely thin during daytime when the GOCI images were captured [8]. The error in the sea ice thickness inversion in the Bohai Sea was ~15% compared to the results of the field survey [15,54].

Sea ice thickness was estimated using Equation (1), in which the shortwave broadband albedo α_h was directly derived from GOCI data. α_h was evaluated using the linear regression model reported previously [55]:

$$\begin{aligned}\alpha_h = &-0.1356\alpha_1 - 0.2704\alpha_2 + 1.4087\alpha_3 - 0.3284\alpha_4 - 0.0812\alpha_5 \\ &+ 0.6204\alpha_6 - 0.1474\alpha_7 - 0.0268\alpha_8 - 0.0464,\end{aligned} \quad (2)$$

where α_j (j = 1, 2, . . . , 8) is the GOCI's reflectance of band *j*.

3.5. Meteorological Parameters

Sea ice formation is strongly related to the period of surface air temperature remaining below or above the freezing/melting point of the seawater, which can be quantified by CFDD and CMDD, respectively [5,14,58]. The mathematical definitions of the two meteorological parameters are as follows:

$$\mathrm{CFDD} = \int_{t=d_s}^{t=d_e} (T_f - T_a)dt, \quad (3)$$

$$\mathrm{CMDD} = \int_{t=d_s}^{t=d_e} (T_a - T_m)dt. \quad (4)$$

where T_f and T_m are the freezing and melting point of the seawater in the Bohai Sea, respectively; T_a is the average daily air temperature of the 13 meteorological stations around the Bohai Sea; t is time in days; and d_s and d_e are the start and end date, respectively. Here, T_f and T_m were set to −2.0 °C and 0 °C, respectively, which are compatible with the salinity in the Bohai Sea (30 PSU) [14].

4. Results

4.1. Sea Ice Area

4.1.1. Validation

The sea ice area extracted on 22 December 2012 was validated using the TM data with a much higher spatial resolution (30 m), and compared to results obtained from the MODIS data with a spatial resolution of 500 m. The extracted sea ice areas from these three datasets were shown to compare well overall with each other (Figure 3). The overall distributions of the Bohai Sea ice from TM, GOCI, and MODIS were comparable. Specifically, the main ice zone in Northern Liaodong Bay and the small individual ice floes in Western Liaodong Bay were all well captured. The sea ice area extracted from both GOCI and MODIS data tend to be overestimated compared to TM data—the sea ice area extracted from the TM data is 3.93×10^3 km^2, whereas those extracted from the GOCI and MODIS data are 4.05×10^3 km^2 and 4.12×10^3 km^2, respectively. The associated mean relative biases of the GOCI and MODIS results are 3.1% and 4.7%, respectively, which suggests that the results of the sea ice area extracted from both GOCI and MODIS data are relatively accurate. The main difference of sea ice distribution lies along the ice edge, which can be better resolved by the TM data with much higher resolution. The lower spatial resolution of the GOCI and MODIS data tended to misclassify some ice–water mixed pixels as sea ice or water, and the estimated sea ice coverage is thus associated with larger error bar compared to TM data.

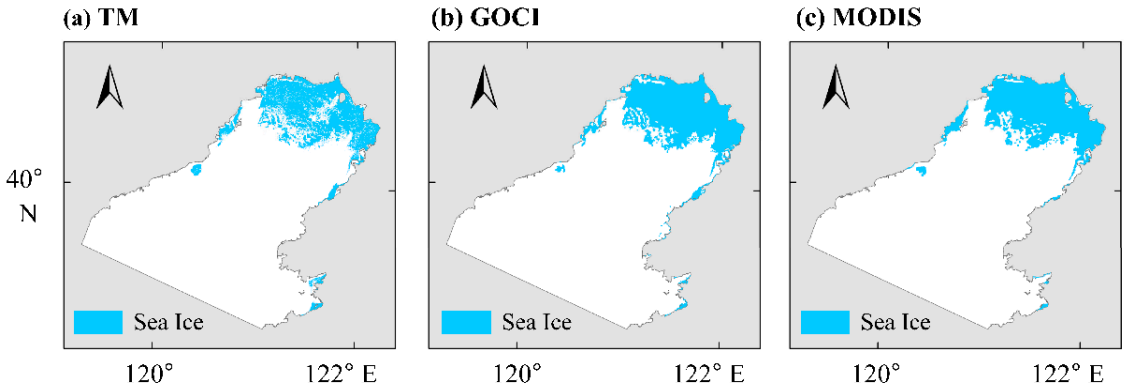

Figure 3. Comparison of sea ice area extracted from (**a**) Landsat Thematic Mapper (TM), (**b**) geostationary ocean color imager (GOCI), and (**c**) moderate resolution imaging spectroradiometer (MODIS) data on 22 December 2012.

4.1.2. Spatiotemporal Distribution and Evolution

The spatiotemporal distribution and evolution of the Bohai Sea ice area during the winter of 2012–2013 are shown in Figure 4. The sea ice first started to appear on the northeastern coastline, then gradually clung to the shore, and further expanded from the shore to the central basin. Among the different bays of the Bohai Sea, the sea ice first appeared and expanded quickly in Liaodong Bay, then expanded southward to Bohai Bay and Laizhou Bay. A significant increase was observed in mid-January 2013, which was followed by a shrinking in late January to early February, and an expansion again in early February. Particularly, on 8 February 2013, Liaodong Bay was almost covered with ice, and the total sea ice area reached its maximum in the entire study period. Starting mid-February, the sea ice area quickly shrunk due to melting. The melting process appeared to be spatially heterogeneous, as a higher melting rate was observed in the Northwestern and Eastern Liaodong Bay compared to other parts of the Bohai Sea. The ice was not completely melted until mid-March. Throughout the entire freezing–melting process, the sea ice was mainly concentrated in Liaodong Bay. The total freezing period in Liaodong Bay was 104 days, whereas in Bohai Bay and Laizhou Bay, the freezing periods were 59 and 51 days, respectively.

Some ice-free zones were observed in Liaodong Bay in the severe ice period. During the period of 22–24 January 2013, the average temperature in the Bohai Sea was −6.9 °C, which was lower than the average temperature of the previous three days. The majority of the existing sea ice was drift ice, with strong dynamic behaviours driven by the currents and winds in the Bohai Sea [1,59]. Therefore, the shrinking of the sea ice in Northern Liaodong Bay during this period was more likely due to the relocation of the drift ice along the fringe of the land-fast sea ice rather than melting. On the contrary, the reduction in ice area in Eastern Liaodong Bay during the period of February 16–19 was mainly due to melting. Specifically, during February 16–18, the average temperature was −1.9 °C, which is closer to the melting point of the sea ice compared to the previous days. Especially on February 17, the average temperature was 1.2°C, causing significant melting (the image was missing due to the cloud cover). The ice-free zone froze again as the temperature dropped to −6.2°C on February 19.

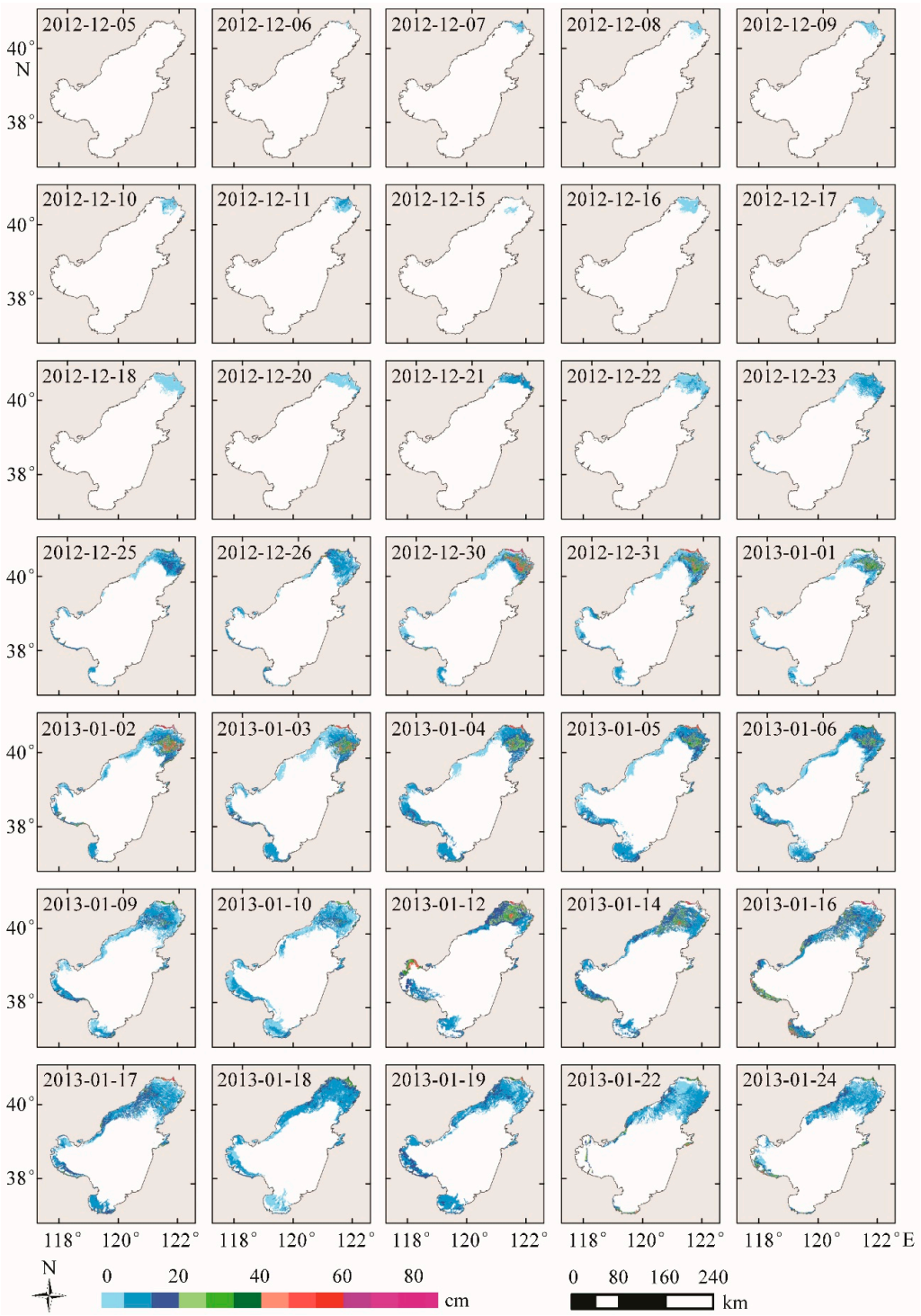

Figure 4. *Cont.*

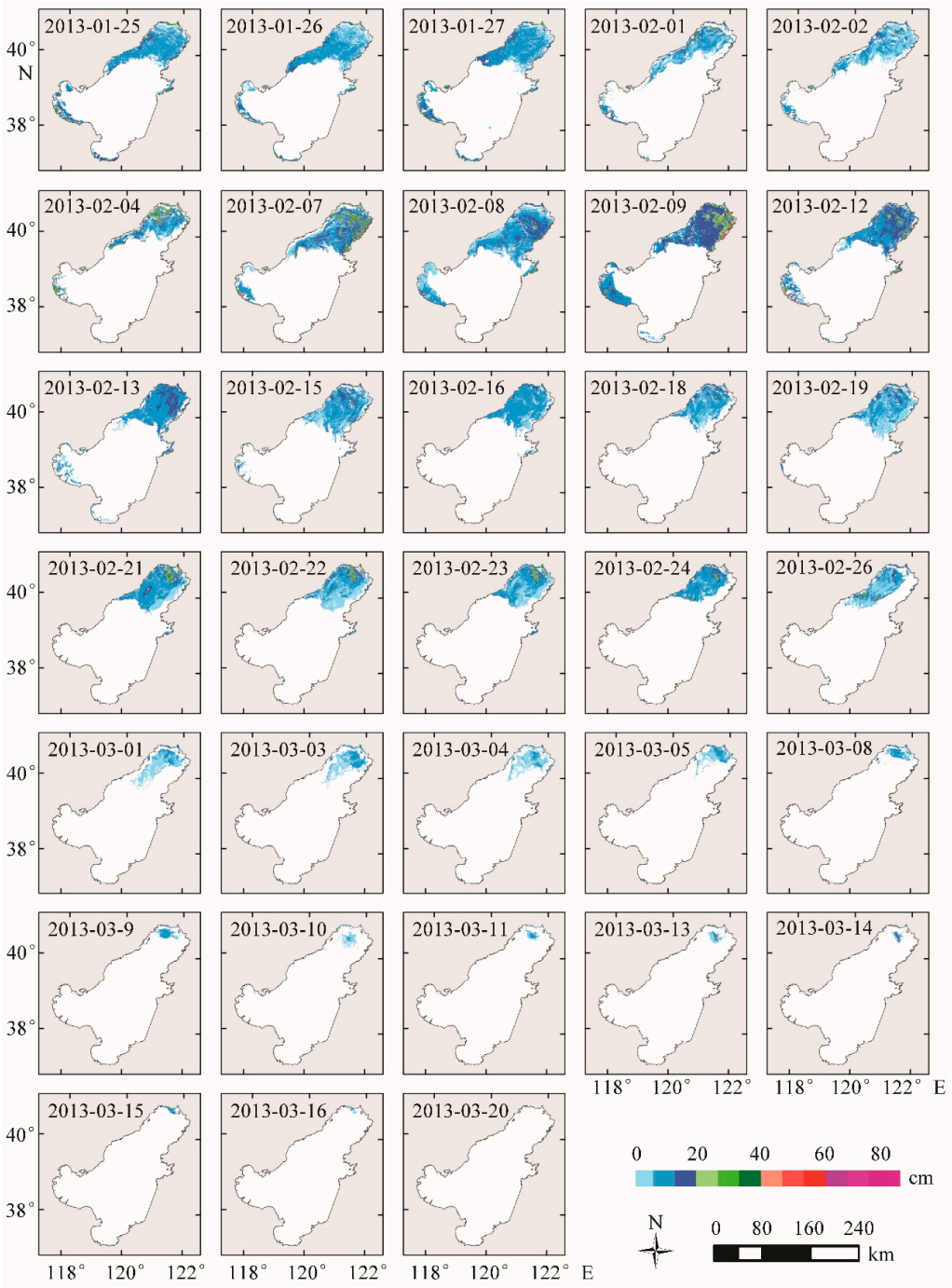

Figure 4. The spatiotemporal distribution and evolution of Bohai Sea ice area and thickness extracted from GOCI data during the winter of 2012–2013.

As seen in Figure 5, the Bohai Sea ice area showed two broad maxima during the entire study period. In late December, sea ice developed rapidly due to a long-term low temperature period, with a mean T_{min} of −13.2 °C. Sea ice area expanded more than four times, from 2.20 × 10^3 km^2 on 21 December 2012 to 9.66 × 10^3 km^2 on 31 December 2012 within 10 days. In early and mid-January 2013, sea ice continued to develop rapidly as the air temperature was maintained below −10 °C, and the sea ice area reached its first peak on January 17 at 17.75 × 10^3 km^2. In late January and early February 2013, sea ice area dropped considerably from 17.16 × 10^3 km^2 on January 27 to 9.74 × 10^3 km^2 on February 4, corresponding to a drastic rise of T_{min} from −12.9 to −0.7 °C in the same period in the Bohai Sea. As of February 5, sea ice expanded once again as the air temperature dropped by ~10 °C

due to a strong cold snap, and the maximum sea ice area of 20.59 × 10^3 km^2 appeared on 8 February, which accounted for 27.9% of the total area of the Bohai Sea. Afterward, sea ice gradually melted as a result of continuous warming.

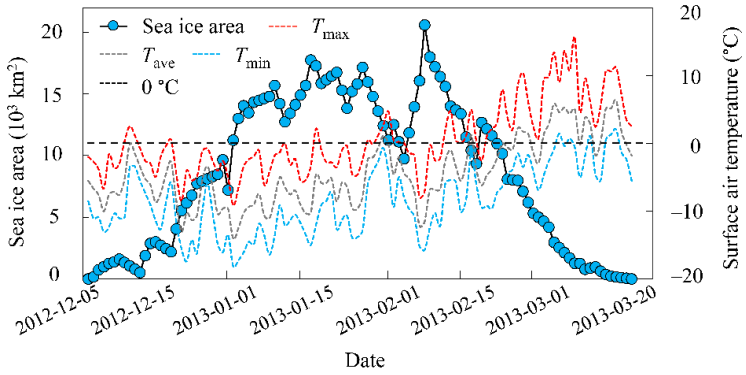

Figure 5. The temporal variation in sea ice area and maximum, average, and minimum daily surface air temperatures (T_{max}, T_{ave}, and T_{min}, respectively) in the Bohai Sea during the winter of 2012–2013.

4.2. Sea Ice Thickness

4.2.1. Validation

The estimated sea ice thickness in the winter of 2012–2013 was validated using in situ observed data available in Karvonen et al. [19]. Figure 6 shows that sea ice thickness estimated from GOCI data mostly falls in the range of variation of the measured data. The overall agreement indicates that sea ice thickness estimated from GOCI data can be effectively used for further analysis. The mean absolute bias of the sea ice thickness retrieved compared to the mean observation value is 4.6 cm, and the root mean square error (RMSE) is 5.8 cm. The estimated thickness in this study is subject to the uncertainty of the prescribed parameters, such as the attenuation coefficient of the albedo (μ_α) in the sea ice thickness inversion formula. Moreover, the discrepancy may be caused by the different scales involved in field measurement and inversion. The ice thickness measured in situ is exactly at the measurement location, whereas the estimated thickness refers to the average over a pixel (500 × 500 m) centered at the measurement location. In addition, the estimated values of sea ice thickness using a sea ice surface heat balance equation introduced by Ouyang et al. (2017) [60] also tended to be on the lower range compared to the observations, with a mean bias of −4.64 cm greater than ours (–1.97 cm).

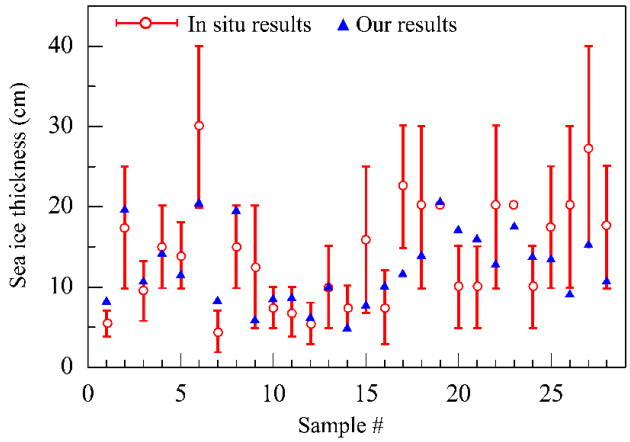

Figure 6. The comparison of sea ice thickness estimated from the GOCI data with the in situ observed ice thickness in the Bohai Sea in the winter of 2012–2013. The red vertical bars represent the range of the in situ observed sea ice thickness, and the blue triangles represent the estimated thickness.

4.2.2. Spatiotemporal Distribution and Evolution

As shown in Figure 4, the spatial distribution of Bohai Sea ice thickness was rather heterogeneous among different bays. Throughout the entire study period, the ice thickness mostly ranged between 0 and 30 cm, except the land-fast ice in Northernmost Liaodong Bay, which reached the maximum thickness of ~90 cm in mid-January. The ice thickness close to the shore in all three bays was usually greater than in the central basin. Generally, average sea ice thickness in Liaodong Bay was greater than that in Bohai Bay, which was in turn larger than that in Laizhou Bay. Within Liaodong Bay, where the most ice occurred, sea ice thickness in the eastern part was generally larger than in the west.

The temporal variation in mean Bohai Sea ice thickness during the study period is further presented in Figure 7. The mean thickness reached the maximum of 19.5 cm on 9 January 2013, and the minimum of 2.5 cm on 15 December 2012. As seen in Figure 7, the mean thickness shows two broad maxima over the entire study period, which is consistent with the temporal pattern of sea ice area. The mean sea ice thickness is best correlated with the mean sea ice area for a two-day lag ($r = 0.76$, $p < 0.01$) based on the lagged correlation analysis.

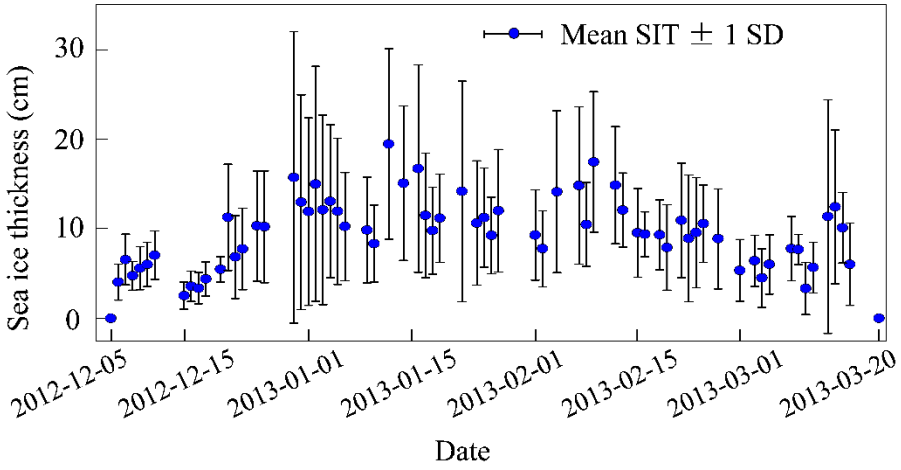

Figure 7. Temporal variation in the estimated mean sea ice thickness (SIT) with one standard deviation (SD, indicated with the vertical bars) in the Bohai Sea in the winter of 2012–2013.

4.3. Correlations Between Sea Ice Characteristics and Meteorological Factors

Due to the Bohai Sea's predominantly shallow water depth, the local synoptic force plays a vital role in sea ice evolution [5,61]. To explore the specific effects of meteorological forcing, correlations between sea ice area/thickness and relevant meteorological factors were examined, including the mean of the daily average and minimum temperature, CFDD, and CMDD of the 13 meteorological stations surrounding Bohai sea in the freezing/melting phase. Weak and moderate negative linear correlations between sea ice area and mean daily average temperature ($r = -0.29$, $p < 0.05$) and minimum temperature ($r = -0.45$, $p < 0.01$) in the freezing phase are shown in Figure 8a,b, respectively, suggesting that the daily temperature is of minor importance in driving sea ice area changes in the freezing process. During the melting phase, strong negative linear correlations between sea ice area and mean daily average temperature ($r = -0.74$, $p < 0.05$) and maximum temperature ($r = -0.63$, $p < 0.01$) are shown in Figure 8d,e, respectively, suggesting that the daily temperature is relatively important for sea ice area changes during the melting process. In Figure 8g,h,j,k, weak/moderate negative linear correlations between sea ice thickness and mean average, minimum, and maximum temperatures during both freezing and melting phases are depicted, which indicate that, compared to sea ice area, sea ice thickness is even less affected by daily temperature.

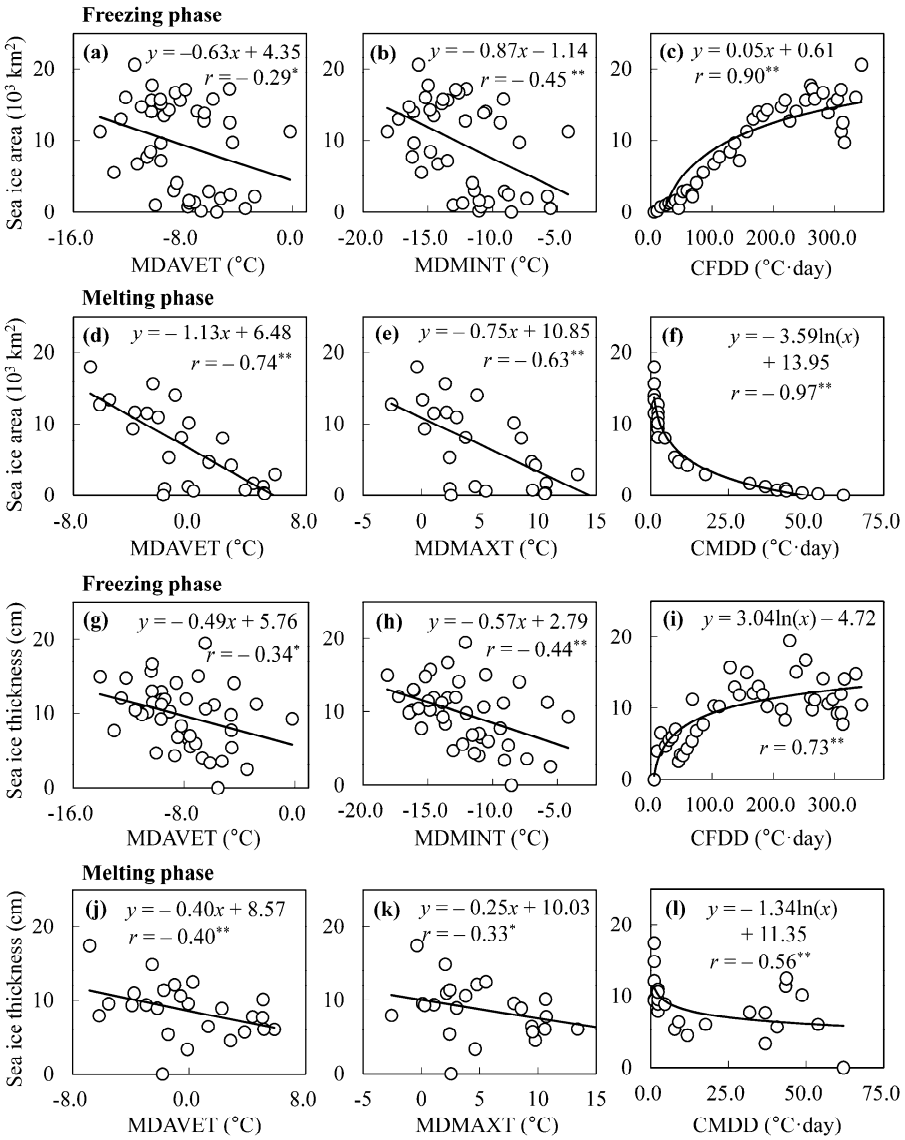

Figure 8. Correlations between sea ice area and (**a**) the mean of the daily average temperature (MDAVET), (**b**) the mean of the daily minimum temperature (MDMINT) of 13 meteorological stations around the Bohai Sea, and the (**c**) cumulative freezing degree days (CFDD) during the freezing phase; correlations between sea ice area and (**d**) MDAVET, (**e**) the mean of the daily maximum temperature (MDMAXT), and (**f**) cumulative melting degree days (CMDD) during the melting phase; correlations between sea ice thickness and (**g**) MDAVET, (**h**) MDMINT, and (**i**) CFDD during the freezing phase; and correlations between sea ice thickness and (**j**) MDAVET, (**k**) MDMAXT, and (**l**) CMDD during the melting phase. The black lines represent the results of regression analysis. * and ** represent significance at the 5% and 1% levels, respectively.

In particular, given the nonlinear correlation between the sea ice area/thickness and the cumulative freezing degree days (CFDD) or cumulative melting degree days (CMDD), logarithmic fitting was tested, and the obtained results were fairly good. There is a very strong positive logarithmic correlation between sea ice area and CFDD ($r = 0.90$, $p < 0.01$, Figure 8c) during the freezing phase, which suggests that CFDD is a controlling factor of the formation of sea ice. During the melting phase, a significant negative logarithmic correlation between sea ice area and CMDD ($r = -0.97$, $p < 0.01$, Figure 8f) was observed, which indicates that CMDD is a crucial parameter controlling sea ice melting. Similarly, a strong logarithmic correlation between sea ice thickness and CFDD ($r = 0.73$, $p < 0.01$, Figure 8i) and a moderate logarithmic correlation between sea ice thickness and CMDD ($r = -0.56$,

$p < 0.01$, Figure 8l) were observed. Overall, we confirmed that the local synoptic forcing, particularly the cumulative parameters, such as CFDD and CMDD, play a vital role in sea ice evolution in the Bohai Sea. This is consistent with some previous studies [62,63]. Therefore, these parameters can be used as indicators for analyzing the evolution of sea ice.

5. Discussion

Our study extends the application of the GOCI data to monitoring of the Bohai Sea ice, and the benefits are multifold. Unlike in situ measurements [19,64], remote sensing-based methods can provide large-scale observation of sea ice for the whole Bohai Sea at a much-reduced cost. Compared with traditional satellite data, such as MODIS, AVHRR, and Sentinel-1A/B, the GOCI data have a fairly high temporal resolution (eight images per day). After removing images with cloud cover, sea fog cover, uneven illumination, and dislocation, GOCI data could provide 68 images to cover 68 days for the frozen season from 5 December 2012 to 20 March 2013 (106 days in total), i.e., temporal coverage of 64.2% (68/106), whereas MODIS could only provide 15 images to cover 15 days for the same period, i.e., temporal coverage of only 14.2% (15/106).

Regarding the sea ice characteristics estimated from the new dataset, the maximum sea ice area during the entire study period was identified as occurring on 8 February 2013, which is consistent with the monitoring result reported in the North China Sea Disaster Bulletin in 2013 (North China Sea Branch of State Oceanic Administration, 2013). However, results from MODIS data showed the maximum on 17 January 2013, as a cloud-free MODIS image was not available on 8 February 2013 [5]. The sea ice area dropped by over 40% from 27 January to 4 February 2013 according to the GOCI data, whereas the MODIS data could not record the detailed changes during this period due to frequent cloud cover. Similarly, the first and last day of the frozen season can be better determined by the GOCI data rather than using MODIS or AVHRR data [5,9]. The proposed approach has more implications for the sea ice hazard risk assessment based on grid computing [1].

In our study, an exponential model [11,14,15,54,55] using GOCI data was used to estimate the ice thickness. The overall agreement between the estimated and in situ observed sea ice thickness indicates that the selected method is reliable. However, some errors still exist due to the limitations of the exponential model and image processing. The exponential model is only suitable for estimating the bare sea ice thickness under snow-free conditions. Although the amount of snowfall in the Bohai Sea in winter is generally minimal [56], snow does still have an impact on the estimation. The uncertainty of the prescribed parameters, such as μ_α, might also cause errors. Yuan (2009) [54] and Yuan et al. (2012) [15] determined the values of μ_α based on in situ observation of sea ice thickness from 2005–2008, which are the most recent results that are available to us and thus adopted in this study. Dedicated frequent in situ observations are recommended in the future to keep up with the rapidly changing environment in the Bohai Sea.The constant μ_α (2.6599), which we assumed for the entire Bohai Sea, is strictly only applicable for Liaodong Bay and Laizhou Bay [15]. However, we consider this a valid assumption, as most of the sea ice coverage is located in Liaodong Bay throughout the ice season. The resultant mean absolute bias of the sea ice thickness retrieved (4.6 cm) is fairly small, which further validated the adopted approach. However, using more regionally specific values of μ_α could still potentially improve the accuracy of the estimated sea ice thickness. When calculating the shortwave broadband albedo (α_h), we did not consider the bi-directional reflectance distribution function (BRDF) effect, as we assumed that the reflection of the sea ice surface is isotropic. However, the reflection of sea ice is actually anisotropic [65]. Without BRDF correction, it is likely to introduce errors in the calculation of α_h [66], which further influences the thickness estimation. Besides, the clouds remaining after the removing process by creating a manual cloud masking may have an influence on the estimation of thickness.

The number of in situ observations for validation of sea ice thickness was limited, which increased the uncertainty of the validation. However, the majority of Bohai Sea ice is drift ice, which is subject to the effects of ocean currents and surface winds, and is hence very dynamic [67]. The number of

observations adds considerable difficulty when conducting large-scale field observations. Development of new technologies for in situ observations in the future will help resolve this limitation.

6. Conclusions

In this study, we monitored the Bohai Sea ice characteristics, including area and thickness, using high-resolution GOCI data during the winter of 2012–2013, during which severe sea ice conditions were recorded. The correlations between sea ice characteristics and potential meteorological factors that may influence the evolution of sea ice were explored. The major findings from the present study are summarized as follows:

The sea ice area extracted from GOCI data was validated using TM data. The temporal variation in sea ice area during the entire study period exhibited two broad maxima. The sea ice thickness estimated from GOCI data was consistent with the in situ observations, and its mean ranged from 2.5 to 19.5 cm with two similar broad maxima.

Spatial distribution within the Bohai Sea showed that sea ice formed and expanded from north to south during the freezing phase, and the opposite occurred for melting. Among the different bays of the Bohai Sea, both sea ice area and thickness in Liaodong Bay were greater than in Bohai Bay, which were in turn greater than in Laizhou Bay.

Correlation analysis suggests that CFDD and CMDD are the dominant meteorological factors driving the change in sea ice area and thickness, whereas daily temperature plays a minor role, particularly for sea ice thickness.

Author Contributions: Conceptualization, Y.Y. and D.S.; methodology, Y.Y. and D.S.; data curation, Y.Y. and K.H.; formal analysis, Y.Y. and K.H.; validation, Y.Y. and K.H.; visualization, Y.Y. and K.H.; writing—original draft preparation, Y.Y.; writing—review and editing, D.S. and Y.X.; supervision, D.S.; project administration, W.G.; funding acquisition, Y.X. and W.G.

Funding: This work was funded by the National Natural Science Foundation of China (41571510), the China Scholarship Council (CSC), and the Open Project Program of the Key Laboratory of Environmental Change and Natural Disaster, Ministry of Education.

Acknowledgments: We thank the Korea Ocean Satellite Center, NASA LAADS, USGS, and Geospatial Data Cloud for providing GOCI, TM, and MODIS data.

Conflicts of Interest: The authors declare no conflict of interest.

References

1. Gu, W.; Liu, C.Y.; Yuan, S.; Li, N.; Chao, J.L.; Li, L.T.; Xu, Y.J. Spatial distribution characteristics of sea-ice-hazard risk in Bohai, China. *Ann. Glaciol.* **2013**, *54*, 73–79. [CrossRef]
2. Gong, D.Y.; Kim, S.J.; Ho, C.H. Arctic Oscillation and ice severity in the Bohai Sea, East Asia. *Int. J. Climatol.* **2007**, *27*, 1287–1302. [CrossRef]
3. Bai, X.Z.; Wang, J.; Liu, Q.Z.; Wang, D.X.; Liu, Y. Severe ice conditions in the Bohai Sea, China, and mild ice conditions in the great lakes during the 2009/10 winter: Links to El Nino and a strong negative arctic oscillation. *J. Appl. Meteorol. Clim.* **2011**, *50*, 1922–1935. [CrossRef]
4. Simmonds, I. Comparing and contrasting the behaviour of Arctic and Antarctic sea ice over the 35-year period 1979–2013. *Ann. Glaciol.* **2015**, *56*, 18–28. [CrossRef]
5. Yan, Y.; Shao, D.; Gu, W.; Liu, C.Y.; Li, Q.; Chao, J.L.; Tao, J.; Xu, Y.J. Multidecadal anomalies of Bohai Sea ice cover and potential climate driving factors during 1988–2015. *Environ. Res. Lett.* **2017**, *12*, 094014. [CrossRef]
6. Tao, S.S.; Dong, S.; Wang, Z.F.; Soares, C.G. Intensity division of the sea ice zones in China. *Cold Reg. Sci. Technol.* **2018**, *151*, 179–187. [CrossRef]
7. Zhang, X.L.; Zhang, Z.H.; Xu, Z.J.; Li, G.; Sun, Q.; Hou, X.J. Sea ice disasters and their impacts since 2000 in Laizhou Bay of Bohai Sea, China. *Nat. Hazards* **2013**, *65*, 27–40. [CrossRef]
8. Gu, W.; Lin, Y.B.; Xu, Y.J.; Yuan, S.; Tao, J.; Li, L.T.; Liu, C.Y. Sea ice desalination under the force of gravity in low temperature environments. *Desalination* **2012**, *295*, 11–15. [CrossRef]
9. Liu, C.Y.; Gu, W.; Chao, J.L.; Li, L.T.; Yuan, S.; Xu, Y.J. Spatio-temporal characteristics of the sea-ice volume of the Bohai Sea, China, in winter 2009/10. *Ann. Glaciol.* **2013**, *54*, 97–104. [CrossRef]

10. Tao, J.; Xu, Y.J.; Zhang, H.; Gu, W. The effect of brackish ice mulching on soil salinity content and crop emergence in man-made, raised bed on saline soils. *Eurasian Soil Sci.* **2018**, *51*, 658–663. [CrossRef]
11. Xie, F.; Wei, G.U.; Yuan, Y.; Chen, Y.H. Estimation of sea ice resources in Liaodong gulf using remote sensing. *Resour. Sci.* **2003**, *25*, 17–23. (In Chinese)
12. Ning, L.; Xie, F.; Gu, W.; Xu, Y.J.; Huang, S.Q.; Yuan, S.; Cui, W.J.; Levy, J. Using remote sensing to estimate sea ice thickness in the Bohai Sea, China based on ice type. *Int. J. Remote Sens.* **2009**, *30*, 4539–4552. [CrossRef]
13. Shi, W.; Wang, M.H. Sea ice properties in the Bohai Sea measured by MODIS-Aqua: 2. Study of sea ice seasonal and interannual variability. *J. Mar. Syst.* **2012**, *95*, 41–49. [CrossRef]
14. Su, H.; Wang, Y.P. Using MODIS data to estimate sea ice thickness in the Bohai Sea (China) in the 2009–2010 winter. *J. Geophys. Res.* **2012**, *117*, C10018. [CrossRef]
15. Yuan, S.; Gu, W.; Xu, Y.J.; Wang, P.; Huang, S.Q.; Le, Z.Y.; Cong, J.O. The estimate of sea ice resources quantity in the Bohai Sea based on NOAA/AVHRR data. *Acta Oceanol. Sin.* **2012**, *31*, 33–40. [CrossRef]
16. Yuan, S.; Liu, C.Y.; Liu, X.Q. Practical model of sea ice thickness of Bohai Sea based on MODIS data. *Chin. Geogr. Sci.* **2018**, *28*, 863–872. [CrossRef]
17. Liu, C.; Chao, J.L.; Gu, W.; Xu, Y.J.; Xie, F. Estimation of sea ice thickness in the Bohai Sea using a combination of VIS/NIR and SAR images. *GISci. Remote Sens.* **2015**, *52*, 115–130. [CrossRef]
18. Zhang, X.; Dierking, W.; Zhang, J.; Meng, J.M. A polarimetric decomposition method for ice in the Bohai Sea using C-band PolSAR data. *IEEE J. Sel. Top. Appl. Earth Obs. Remote Sens.* **2015**, *8*, 47–66. [CrossRef]
19. Karvonen, J.; Shi, L.J.; Cheng, B.; Simila, M.; Makynen, M.; Vihma, T. Bohai Sea ice parameter estimation based on thermodynamic ice model and Earth observation data. *Remote Sens.* **2017**, *9*, 234. [CrossRef]
20. Dierking, W. Sea ice monitoring by synthetic aperture radar. *Oceanography* **2013**, *26*, 100–111. [CrossRef]
21. Choi, J.K.; Park, Y.J.; Ahn, J.H.; Lim, H.S.; Eom, J.; Ryu, J.H. GOCI, the world's first geostationary ocean color observation satellite, for the monitoring of temporal variability in coastal water turbidity. *J. Geophys. Res.* **2012**, *117*, C09004. [CrossRef]
22. Ryu, J.H.; Han, H.J.; Cho, S.; Park, Y.J.; Ahn, Y.H. Overview of geostationary ocean color imager (GOCI) and GOCI data processing system (GDPS). *Ocean Sci. J.* **2012**, *47*, 223–233. [CrossRef]
23. Amin, R.; Shulman, I. Hourly turbidity monitoring using Geostationary Ocean Color Imager fluorescence bands. *J. Appl. Remote Sens.* **2015**, *9*, 096024. [CrossRef]
24. Mao, Y.; Wang, S.Q.; Qiu, Z.F.; Sun, D.Y.; Bilal, M. Variations of transparency derived from GOCI in the Bohai Sea and the Yellow Sea. *Opt. Express* **2018**, *26*, 12191–12209. [CrossRef] [PubMed]
25. Yang, H.; Choi, J.K.; Park, Y.J.; Han, H.J.; Ryu, J.H. Application of the Geostationary Ocean Color Imager (GOCI) to estimates of ocean surface currents. *J. Geophys. Res.* **2014**, *119*, 3988–4000. [CrossRef]
26. Hu, Z.F.; Wang, D.P.; Pan, D.L.; He, X.Q.; Miyazawa, Y.; Bai, Y.; Wang, D.F.; Gong, F. Mapping surface tidal currents and Changjiang plume in the East China Sea from geostationary ocean color imager. *J. Geophys. Res.* **2016**, *121*, 1563–1572. [CrossRef]
27. Jiang, L.D.; Wang, M.H. Diurnal currents in the Bohai Sea derived from the Korean geostationary ocean color imager. *IEEE Trans. Geosci. Remote Sens.* **2017**, *55*, 1437–1450. [CrossRef]
28. Park, K.A.; Lee, M.S.; Park, J.E.; Ullman, D.; Cornillon, P.C.; Park, Y.J. Surface currents from hourly variations of suspended particulate matter from Geostationary Ocean Color Imager data. *Int. J. Remote Sens.* **2018**, *39*, 1929–1949. [CrossRef]
29. Yeom, J.M.; Kim, H.O. Comparison of NDVI from GOCI and MODIS data towards improved assessment of crop temporal dynamics in the case of paddy rice. *Remote Sens.* **2015**, *7*, 11326–11343. [CrossRef]
30. Sun, D.Y.; Huan, Y.; Qiu, Z.F.; Hu, C.M.; Wang, S.Q.; He, Y.J. Remote-sensing estimation of phytoplankton size classes from GOCI satellite measurements in Bohai Sea and Yellow Sea. *J. Geophys. Res.* **2017**, *122*, 8309–8325. [CrossRef]
31. Lee, E.A.; Kim, S.Y. Regional variability and turbulent characteristics of the satellite-sensed submesoscale surface chlorophyll concentrations. *J. Geophys. Res.* **2018**, *123*, 4250–4279. [CrossRef]
32. Ruddick, K.; Vanhellemont, Q.; Yan, J.; Neukermans, G.; Wei, G.M.; Shang, S.L. Variability of suspended particulate matter in the Bohai Sea from the Geostationary Ocean Color Imager (GOCI). *Ocean Sci. J.* **2012**, *47*, 331–345. [CrossRef]
33. Huang, C.C.; Li, Y.M.; Liu, G.; Guo, Y.L.; Yang, H.; Zhu, A.X.; Song, T.; Huang, T.; Zhang, M.L.; Shi, K. Tracing high time-resolution fluctuations in dissolved organic carbon using satellite and buoy observations: Case study in Lake Taihu, China. *Int. J. Appl. Earth Obs.* **2017**, *62*, 174–182. [CrossRef]

34. Pan, Y.Q.; Shen, F.; Wei, X.D. Fusion of Landsat-8/OLI and GOCI data for hourly mapping of suspended particulate matter at high spatial resolution: A case study in the Yangtze (Changjiang) Estuary. *Remote Sens.* **2018**, *10*, 158. [CrossRef]
35. Choi, J.K.; Min, J.E.; Noh, J.H.; Han, T.H.; Yoon, S.; Park, Y.J.; Moon, J.E.; Ahn, J.H.; Ahn, S.M.; Park, J.H. Harmful algal bloom (HAB) in the East Sea identified by the Geostationary Ocean Color Imager (GOCI). *Harmful Algae* **2014**, *39*, 295–302. [CrossRef]
36. Lou, X.L.; Hu, C.M. Diurnal changes of a harmful algal bloom in the East China Sea: Observations from GOCI. *Remote Sens. Environ.* **2014**, *140*, 562–572. [CrossRef]
37. Liu, R.J.; Zhang, J.; Yao, H.Y.; Cui, T.W.; Wang, N.; Zhang, Y.; Wu, L.J.; An, J.B. Hourly changes in sea surface salinity in coastal waters recorded by Geostationary Ocean Color Imager. *Estuar. Coast Shelf. Sci.* **2017**, *196*, 227–236. [CrossRef]
38. Yuan, Y.B.; Qiu, Z.F.; Sun, D.Y.; Wang, S.Q.; Yue, X.Y. Daytime sea fog retrieval based on GOCI data: A case study over the Yellow Sea. *Opt. Express* **2016**, *24*, 787–801. [CrossRef]
39. Korea Ocean Satellite Center (KOSC). Available online: http://kosc.kiost.ac.kr/eng/ (accessed on 1 July 2018).
40. U.S. Geological Survey (USGS). Available online: https://www.usgs.gov/ (accessed on 21 August 2018).
41. Geospatial Data Cloud Website. Available online: http://www.gscloud.cn/ (accessed on 21 August 2018).
42. National Aeronautics and Space Administration (NASA). Level 1 and Atmosphere Archive and Distribution System (LAADS). Available online: https://ladsweb.modaps.eosdis.nasa.gov/ (accessed on 21 August 2018).
43. National Meteorological Information Center of China. Available online: http://data.cma.cn/ (accessed on 30 August 2018).
44. Du, C.G.; Li, Y.M.; Wang, Q.; Liu, G.; Zheng, Z.B.; Mu, M.; Li, Y. Tempo-spatial dynamics of water quality and its response to river flow in estuary of taihu lake based on GOCI imagery. *Environ. Sci. Pollut. Res.* **2017**, *24*, 28079–28101. [CrossRef]
45. Pope, E.L.; Willis, I.C.; Pope, A.; Miles, E.S.; Arnold, N.S.; Rees, W.G. Contrasting snow and ice albedos derived from MODIS, Landsat ETM+ and airborne data from Langjokull, Iceland. *Remote Sens. Environ.* **2016**, *175*, 183–195. [CrossRef]
46. Legleiter, C.J.; Tedesco, M.; Smith, L.C.; Behar, A.E.; Overstreet, B.T. Mapping the bathymetry of supraglacial lakes and streams on the Greenland ice sheet using field measurements and high-resolution satellite images. *Cryosphere* **2014**, *8*, 215–228. [CrossRef]
47. Wunderground. Available online: https://www.wunderground.com/ (accessed on 5 July 2018).
48. Myint, S.W.; Gober, P.; Brazel, A.; Grossman-Clarke, S.; Weng, Q. Per-pixel vs. object-based classification of urban land cover extraction using high spatial resolution imagery. *Remote Sens. Environ.* **2011**, *115*, 1145–1161. [CrossRef]
49. Zhao, Z.Y.; Liu, Z.; Gong, P. Automatic extraction of floating ice at Antarctic continental margin from remotely sensed imagery using object-based segmentation. *Sci. China Earth Sci.* **2012**, *55*, 622–632. [CrossRef]
50. Miao, X.; Xie, H.J.; Ackley, S.F.; Perovich, D.K.; Ke, C.Q. Object-based detection of arctic sea ice and melt ponds using high spatial resolution aerial photographs. *Cold Reg. Sci. Technol.* **2015**, *119*, 211–222. [CrossRef]
51. Wakabayashi, H.; Mori, Y.; Nakamura, K. Sea ice detection in the sea of Okhotsk using PALSAR and MODIS data. *IEEE J. Sel. Top. Appl. Earth Obs. Remote Sens.* **2013**, *6*, 1516–1523. [CrossRef]
52. Grenfell, T.C. A radiative transfer model for sea ice with vertical structure variations. *J. Geophys. Res.* **1991**, *96*, 16991–17001. [CrossRef]
53. Gardner, A.S.; Sharp, M.J. A review of snow and ice albedo and the development of a new physically based broadband albedo parameterization. *J. Geophys. Res.* **2010**, *115*, F01009. [CrossRef]
54. Yuan, S. The Space-Time Distribution of Sea Ice Resource Quantity in Bohai Sea and Its Response to Climate Change. Ph.D. Thesis, Beijing Normal University, Beijing, China, 2009.
55. Liu, W.S.; Sheng, H.; Zhang, X. Sea ice thickness estimation in the Bohai Sea using geostationary ocean color imager data. *Acta Oceanol. Sin.* **2016**, *35*, 105–112. [CrossRef]
56. Yang, G.J. *Sea Ice Engineering*; China Petroleum Industry Press: Beijing, China, 2000; pp. 455–480. (In Chinese)
57. Yuan, S.; Gu, W.; Liu, C.Y.; Xie, F. Towards a semi-empirical model of the sea ice thickness based on hyperspectral remote sensing in the Bohai Sea. *Acta Oceanol. Sin.* **2017**, *36*, 80–89. [CrossRef]

58. Tamura-Wicks, H.; Toumi, R.; Budgell, W.P. Sensitivity of caspian sea-ice to air temperature. *Q. J. R. Meteorol. Soc.* **2015**, *141*, 3088–3096. [CrossRef]
59. Wu, L.T.; Wu, H.D.; Li, W.B.; Liu, Q.Z.; Zhang, Y.F.; Liu, Y.; Bai, S. Sea ice drifts in response to winds and tide in the Bohai Sea. *Acta Oceanol. Sin.* **2005**, *27*, 15–21. (In Chinese)
60. Ouyang, L.X.; Hui, F.M.; Zhu, L.X.; Cheng, X.; Cheng, B.; Shokr, M.; Zhao, J.C.; Ding, M.H.; Zeng, T. The spatiotemporal patterns of sea ice in the Bohai Sea during the winter seasons of 2000–2016. *Int. J. Digit. Earth* **2017**. [CrossRef]
61. Wassermann, S.; Schmitt, C.; Kottmeier, C.; Simmonds, I. Coincident vortices in Antarctic wind fields and sea ice motion. Geophysical research letters. *Geophys. Res. Lett.* **2006**, *33*, L15810. [CrossRef]
62. Zhang, N.; Wu, Y.S.; Zhang, Q.H. Forecasting the evolution of the sea ice in the Liaodong Bay using meteorological data. *Cold Reg. Sci. Technol.* **2016**, *125*, 21–30. [CrossRef]
63. Comiso, J.C.; Gersten, R.A.; Stock, L.V.; Turner, J.; Perez, G.J.; Cho, K. Positive trend in the Antarctic sea ice cover and associated changes in surface temperature. *J. Clim.* **2017**, *30*, 2251–2267. [CrossRef]
64. Zeng, T.; Shi, L.J.; Marko, M.; Cheng, B.; Zou, J.H.; Zhang, Z.P. Sea ice thickness analyses for the Bohai Sea using MODIS thermal infrared imagery. *Acta Oceanol. Sin.* **2016**, *35*, 96–104. [CrossRef]
65. Xu, Z.T.; Yang, Y.Z.; Wang, G.F.; Cao, W.X.; Kong, X.P. Reflectance of Sea Ice in Liaodong Bay. *Spectrosc. Spect. Anal.* **2010**, *30*, 1902–1907. (In Chinese)
66. Li, F.; Jupp, D.L.; Reddy, S.; Lymburner, L.; Mueller, N.; Tan, P.; Islam, A. An evaluation of the use of atmospheric and BRDF correction to standardize Landsat data. *IEEE J. Sel. Top. Appl. Earth Obs. Remote Sens.* **2010**, *3*, 257–270. [CrossRef]
67. Shi, W.Q.; Yuan, S.; Xu, N.; Chen, W.B.; Liu, Y.Q.; Liu, X.Q. Analysis of floe velocity characteristics in small-scaled zone in offshore waters in the eastern coast of Liaodong Bay. *Cold Reg. Sci. Technol.* **2016**, *126*, 82–89. [CrossRef]